18th Brazilian Congress of Thermal Sciences and Engineering
November 16-20, 2020 (Online)

ENC-2020-0562
COMPARISON OF THE EXPERIMENTAL PERFORMANCE OF A THERMOSYPHON WITH ITS THERMAL DESIGN

Pedro Leineker Ochoski Machado[1*]
Rogério de Oliveira Souza[1]
Romeu Miqueias Szmoski[2]
Thiago Antonini Alves[1]
Federal University of Technology – Paraná, [1]Academic Department of Mechanics, [2]Academic Department of Physics
Rua Doctor Washington Subtil Chueire, 330, Jardim Carvalho, 84017-220, Ponta Grossa, PR, Brazil
pedmac@alunos.utfpr.edu.br*, rogerio.2016@alunos.utfpr.edu.br, rmszmoski@gmail.com, antonini@utfpr.edu.br

Vitor Otávio Ochoski Machado[3]
Federal University of Technology – Paraná, [3]Academic Department of Mechanics
Deputado Heitor Alencar Furtado street, 5000, Ecoville, 81280-340, Curitiba, PR, Brasil
vitmac@alunos.utfpr.edu.br

Abstract. *A thermosyphon is a gravity-assisted heat pipe used to improve heat transfer in several applications. Its main feature is the use of latent heat of vaporization to transmit heat at high rates over considerable distances with a small decrease in temperature. In this work, the experimental performance of a thermosyphon was compared with its thermal design, in order to verify its correct operating. The thermosyphon was manufactured from a copper tube with an outer diameter of 22.23mm, an inner diameter of 20.80mm, and a total length of 840mm. The working fluid used was distilled water with a filling ratio of 50% of the evaporator volume. The evaporator has a length of 650mm, while the adiabatic section and condenser have lengths of 80mm and 110mm, respectively. The condenser was cooled by water forced convection and the evaporator was heated by Joule's effect. Experimental tests were performed for a heat load of 80 to 140W in a position at 25º from the horizontal (evaporator above the condenser). The thermal analysis of the thermosyphon was performed from thermocouples arranged in their regions, as well as the value of the thermal load dissipated by it. Some specific points of the experimental apparatus were identified for possible adjustments, such as better insulation, different manifold, and different water flow conditions. The thermosyphon operated as expected in all the analyzed aspects – temperature distribution, thermal resistance, thermal design's heat load, and thermal and exergy efficiencies – which showed that the methodology used to its construction is adequate.*

Keywords: *Thermosyphon, Heat pipe, Experimental, Thermal design.*

1. INTRODUCTION

A thermosyphon is a gravity-assisted heat pipe used to improve heat transfer in several applications. The main feature of a thermosyphon is the use of latent heat of vaporization to transmit heat at high rates over considerable distances with a small decrease in temperature. Its advantages are flexibility, simple construction, and easy control without external pumping power (Akbasrzadeh and Wadowski, 1996).

Both a thermosyphon and a heat pipe basically consist of a hollow, evacuated metal pipe, where a certain amount of working fluid is inserted. The main difference from a thermosyphon to a heat pipe is that the heat pipe is lined internally by a porous structure that is intended to carry the working fluid, whereas the means of transporting the thermosyphon fluid is based on pressure gradients and in the action of gravity (Reay et al., 2014).

A thermosyphon has three regions with different functions in its operation. These regions are called evaporator, adiabatic section, and condenser. The evaporator, the lower part of the tube, is heated by a hot source and the working fluid is submitted to a boiling process. The steam generated, due to the pressure difference, moves to the coldest region, which is in the upper region of the tube (condenser). In the condenser, the vapor generated in the evaporator loses energy as heat and it is condensed, causing the return of the working fluid in the liquid state to the evaporator by gravity, closing the thermodynamic cycle. The adiabatic section is located between the evaporator and the condenser. In this section, there is no heat transfer between the thermosyphon and the environment. In some cases, the adiabatic section is absent (Mantelli, 2013). A schematic diagram of the thermosyphon operating principle is shown in Fig. 1.

Thermosyphons can be widely applied in the industrial environment. An application example is heat recovery in an exhaust gas system, preheating the air in boiler heat exchangers. They are also widely used in places of extreme cold to exchange heat with the hottest part of the soil, and can assist in keeping roads operating in winter and even heating environments. In addition, in cold regions containing oil transport lines, the thermosyphons act by capturing heat from the oil in the tube and transferring it to the external environment, reducing the heat that the base receives and transfers to the soil, thus preventing thawing and instability of the foundation. Thermosyphons are also used in vacuum solar collectors, which are highly effective and applicable for heating water for daily use, environments and also swimming pools. Another area of application is the drying and dehydration of food products and fabrics, in addition to the electronic cooling (Aguiar, 2016).

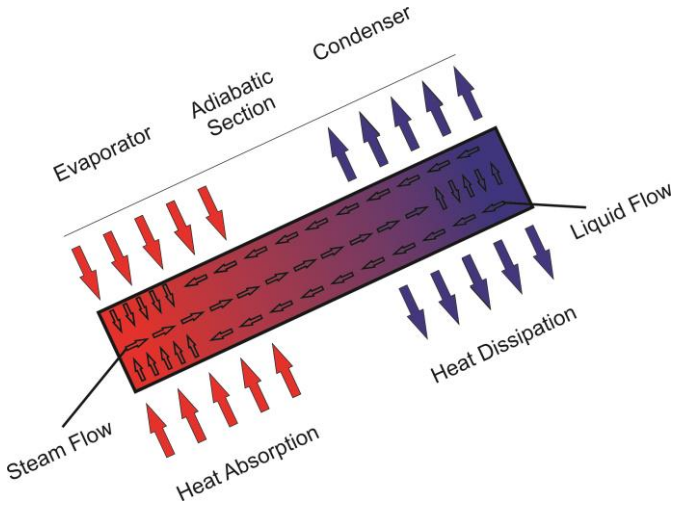

Figure 1. Schematic diagram of a thermosyphon.

In order to verify the proper working of a thermosyphon a thermal analysis can be made, where the use of the thermosyphon submitted to different values of heat loads is simulated and the temperature is checked in all three sections during each test, verifying if the behaviour of this device matches the conditions of its desired application. Another way to do that is to consider the temperature drop between the evaporator and the condenser obtained experimentally and apply it to the thermal design of a thermosyphon, where, with the temperatures of the three sections and external conditions imposed to the evaporator and condenser, it's possible to calculate the thermal charge imposed to the device and verify if it matches with the actual thermal charge imposed in the experiment (Peterson, 1994).

Taking that into account, this present work intends to build a thermosyphon and perform its thermal analysis aiming to verify if the intended device can be used as part of a photovoltaic/thermal (PV/T) hybrid collector system, where the thermosyphon will be used to cool a photovoltaic panel and heat water at the same time. By this, the panel at a lower temperature will generate a higher amount of electricity and also act as a solar collector, heating water, elevating its general energy efficiency and contributing to the environment by producing clean energy, both electrical and thermal. In order to achieve the thermal analysis, experimental data will be verified and compared to the thermal design results.

2. THERMAL DESIGN

The design of a thermosyphon is based in the electrical and thermal circuit analogy, using the concept of thermal resistances (Peterson, 1994). The thermal resistances of a thermosyphon can be seen in Fig. 2, while the thermal load applied to it can be obtained by Eq. (1):

$$\Delta T_a = q_{td} R_{th,design}, \tag{1}$$

in which ΔT_a represents the temperature drop between the evaporator and condenser, $R_{th,design}$ represents the total thermal resistance, and q_{td} is the thermal load calculated from the thermal design.

The total thermal resistance can be obtained using the same concept as electrical resistances association. Taking into account Fig. 2, $R_{th,design}$ can be obtained by Eq. (2).

$$R_{th,design} = R_1 + \left[(R_2 + R_3 + R_4 + R_5 + R_6 + R_7 + R_8)^{-1} + R_{10}^{-1} \right]^{-1} + R_9 . \tag{2}$$

The resistances R_1 and R_9 represent the convection resistance from the evaporator and condenser, respectively (Peterson, 1994). They can be obtained by Eq. (3) and Eq. (4):

$$R_1 = \frac{1}{h_{o,evap} A_{evap}}, \tag{3}$$

$$R_9 = \frac{1}{h_{o,cond} A_{cond}}, \tag{4}$$

in which $h_{o,evap}$ and $h_{o,cond}$ represent the convective coefficient at the evaporator and condenser, respectively, and A_{evap} and A_{cond} represents the external area from the evaporator and condenser, respectively.

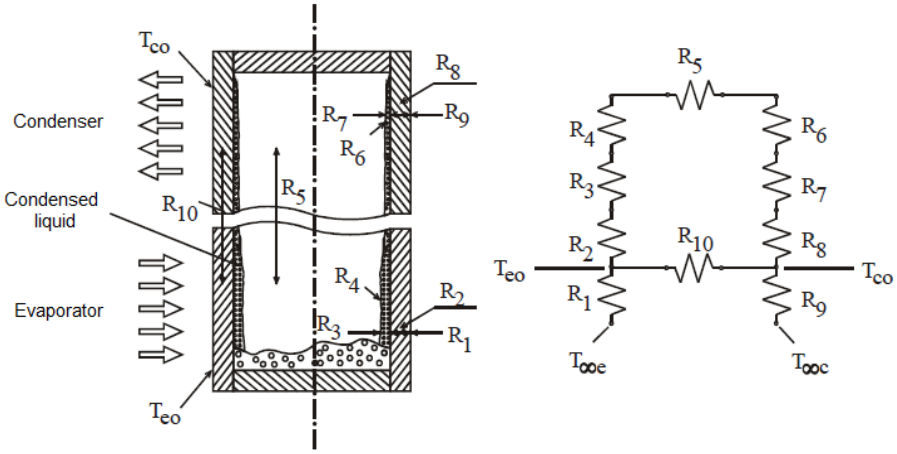

Figure 2. Thermal resistances of a thermosyphon.
Adapted from (Mantelli, 2013).

The resistances R_2 and R_8 represent the conduction resistance from the evaporator and condenser, respectively (Peterson, 1994), in which d_o and d_i represent the outer and inner diameter of the involucre, k_s represents the thermal conductivity of the involucre, and l_{evap} and l_{cond} represent the length of the evaporator and condenser, respectively. They can be obtained by Eq. (5) and Eq. (6).

$$R_2 = \frac{\ln\left(\frac{d_o}{d_i}\right)}{2\pi l_{evap} k_s}, \tag{5}$$

$$R_8 = \frac{\ln\left(\frac{d_o}{d_i}\right)}{2\pi l_{cond} k_s}. \tag{6}$$

The resistances R_3 and R_7 correspond to the thermal resistances referring to the phase change of the working fluid in the evaporator and in the condenser, in that order (Peterson, 1994). The resistance related to boiling in the evaporator must be analyzed in two parts according to Groll and Rösler (1992). The first part corresponds to the evaporation of the liquid film on the sides of the tube (R_{3f} – Eq. (7)) and the second one to the evaporation of the liquid contained in the pool (R_{3p} – Eq. (9)).

$$R_{3f} = \frac{0,345 q_e^{1/3}}{d_i^{4/3} g^{1/3} l_{evap} \varphi_2^{4/3}}, \tag{7}$$

$$\varphi_2 = \left(\frac{h_{lv} k_l^3 \rho_l^2}{\mu_l}\right)^{1/4}, \tag{8}$$

$$R_{3p} = \left(\frac{1}{g^{0,2} \varphi_3 q_e^{0,4} (\pi d_i l_{evap})^{0,6}}\right), \tag{9}$$

$$\varphi_3 = \left(\frac{\rho_l^{0,65} k_l^{0,3} c_{p,l}^{0,7}}{\rho_v^{0,25} h_{lv}^{0,4} \mu_l^{0,1}} \right) \left(\frac{P_v}{P_{atm}} \right)^{0,23} \quad . \tag{10}$$

In Equation (7), q_e represents an estimated heat (Eq. (13)), while in Eq. (8), k_l corresponds to the thermal conductivity of the liquid phase of the working fluid. In Equation (10), $c_{p,l}$ represents the specific heat at the constant pressure of the liquid phase of the fluid, P_v refers to the vapor pressure (obtained at the saturation temperature T_v - Eq. (16)), and P_{atm} corresponds to the atmospheric pressure. Also, ρ_l and ρ_v, μ_l and μ_v represent the density and viscosity of the liquid and gas phases, respectively, while h_{lv} represents the enthalpy of vaporization of the fluid. All of them should be taken at T_v.

The value of R_3 can then be obtained by Eq. (11), where FR corresponds to the thermosyphon filling ratio, which consists of the ratio between the volume of working fluid V_l and the volume of the evaporator V_{evap}, as can be seen in Eq. (12) (Peterson, 1994).

$$R_3 = R_{3p}\, FR + (1 - FR)\, R_{3f} \,, \tag{11}$$

$$FR = \frac{V_l}{V_{evap}} \,, \tag{12}$$

$$q_e = \frac{\Delta T_a}{(R_1 + R_2 + R_8 + R_9)} \,. \tag{13}$$

In Equation (14), $T_{\infty e}$ and $T_{\infty c}$ represent the external fluid temperature at the evaporator and the condenser, respectively, whereas ΔT_h corresponds to the difference in average hydrostatic temperature in the thermosyphon, which is determined by Eq. (15). The steam temperature is represented by T_v (saturation temperature - Eq. (16)) and T_p represents the temperature of the pool, which is obtained through the pressure of the pool P_p - Eq. (17), where g is the gravity acceleration and β is the inclination angle of the thermosyphon. The resistance R_7 can be determined by Eq. (18) (Peterson, 1994).

$$\Delta T_a = (T_{\infty e} - T_{\infty c}) - \Delta T_h \,, \tag{14}$$

$$\Delta T_h = \left(\frac{T_v - T_p}{2} \right) FR \,, \tag{15}$$

$$T_v = T_{\infty c} + \left(\frac{R_8 + R_9}{R_1 + R_2 + R_8 + R_9} \right) \left(T_{\infty e} - T_{\infty c} \right) \,, \tag{16}$$

$$P_p = P_v + \rho_l\, g\, FR\, l_{evap}\, sin(\beta) \,, \tag{17}$$

$$R_7 = \frac{0,345 q_e^{1/3}}{d_i^{4/3} g^{1/3} l_{cond} \varphi_2^{4/3}} \,. \tag{18}$$

The resistance R_{10} represents the thermal resistance of axial conduction throughout the involucre and can be determined by Eq. (19), in which A_t represents the cross-sectional area of the tube, l_a consists in the wet length of the evaporator, and l_{adiab} represents the length of the adiabatic section (Peterson, 1994).

$$R_{10} = \frac{\left[l_{adiab} + 0,5(l_a + l_{cond}) \right]}{A_t k_s} \,. \tag{19}$$

The resistances R_4 and R_6 represent the thermal resistances at the liquid-vapor interface in the evaporator and in the condenser, respectively, while R_5 represents the resistance associated with the drop in saturation temperature between the evaporator and the condenser. Such resistances, when carrying out an analysis of magnitude, appear very small in relation to the other resistances, and can then be neglected in the design of the thermosyphons (Peterson, 1994).

3. METHODOLOGY

This section presents the apparatus and proceedings intended to be used in order to achieve the main goal of this work.

3.1 Experimental Apparatus

The experimental apparatus used in this study is shown in Fig. 3 and was composed of a *Politerm*™16E power supply (A), an *Agilent*™ 34970A data acquisition system with a 20-channel multiplexer (B), a *Solab*™ SL-130 ultra-thermostatic bath (C), a *Dell*™ laptop (D), a UPS *NHS*™ (E), and an *Omega Engineering*™ FL-2051 variable area flowmeter with regulating valve (F).

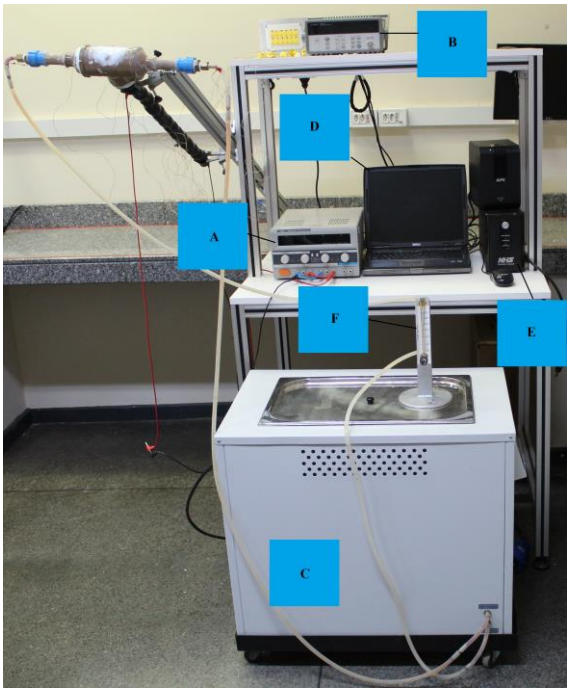

Figure 3. Experimental Apparatus.

3.2 Experimental Procedure

The thermosyphon was manufactured from a copper ASTM B75 tube with an outer diameter of 22.23mm, an inner diameter of 20.80mm, and a total length of 840mm. The working fluid used was distilled water with a filling ratio of 50% of the evaporator volume. The evaporator has a length of 650mm, while the adiabatic section and condenser have lengths of 80mm and 110mm, respectively. The methodology used in the building of the thermosyphons (preparation, cleaning, assembly, tightness test, evacuation procedure, and filling with working fluid) was based on the information provided in Antonini Alves et al. (2018).

A resistive tape was wrapped in the whole length of the evaporator. The tape was also connected with the power supply, allowing the dissipation of its power in the form of heat due to Joule's effect, heating the evaporator. The condenser was placed inside a 60mm diameter polyvinyl chloride tee that acts as a manifold and a water flow of 0.9L/min is responsible for the cooling of the thermosyphon and the condensing of the working fluid. The water used for the cooling process and the ambient temperature are kept at 16.0°C ± 0.5°C by the ultra-thermostatic bath and a *Rhemm*™ air conditioning system, respectively. Experimental tests were carried out for a heat load of 80 to 140W in a position at 25° from the horizontal (evaporator below condenser) corresponding to the latitude of the city of Ponta Grossa/PR/Brazil: 25°05'42" South.

A total of nine *Omega Engineering*™ type K thermocouples were distributed along the thermosyphon, one at the condenser (T_{cond}), one at the adiabatic section (T_{adiab}), and seven at the evaporator ($T_{evap,1}$, $T_{evap,2}$, $T_{evap,3}$, $T_{evap,4}$, $T_{evap,5}$, $T_{evap,6}$, and $T_{evap,7}$). The temperature data were collected every ten seconds using the data acquisition system. Each heat value was kept at the evaporator for about 45 minutes and each test was repeated three times in order to verify the data repeatability.

All the equations from the thermal design were implemented in the *F-Chart*™ software *Engineering Equation Solver*™ (*EES*™) as well as all the experimental parameters used in the experimental test, such as dimensions, materials, filling ratio, and inclination. All the thermodynamic and material properties were taken from *EES*™ database, allowing the calculation of all the thermal resistances and the thermal load of the thermosyphon.

Since there is no convection heat exchange at the evaporator, and a constant heat flux instead, some changes at the thermal design were made. There is no need to calculate R_1, so Eq. (2) can be rewritten as Eq. (20). Equations (14) and (16) also need changes, becoming Eqs. (21) and (22), respectively. T_{eo} represents the external temperature of the evaporator's wall.

$$R_{th,design} = \left[(R_2 + R_3 + R_4 + R_5 + R_6 + R_7 + R_8)^{-1} + R_{10}{}^{-1} \right]^{-1} + R_9 , \tag{20}$$

$$\Delta T_a = (T_{eo} - T_{\infty c}) - \Delta T_h , \tag{21}$$

$$T_v = T_{\infty c} + \left(\frac{R_8 + R_9}{R_2 + R_8 + R_9} \right) (T_{eo} - T_{\infty c}) . \tag{22}$$

The step by step to work with the thermal design of a thermosyphon corresponds to:

#1) Specify the project parameters (l_{evap}, l_{adiab}, l_{cond}, d_o, d_i, β, $h_{o,evap}$, $h_{o,cond}$, FR, k_s, T_{eo}, $T_{\infty e}$, and $T_{\infty c}$);
#2) Calculate R_2 (Eq. (5)), R_8 (Eq. (6)), and R_9 (Eq. (4));
#3) Estimate the vapor temperature T_v (Eq. (16));
#4) Calculate the thermodynamic properties of the working fluid at saturation temperature T_v (P_v, ρ_l, ρ_v, h_{lv}, μ_l, μ_v, k_l and $c_{p,l}$);
#5) Calculate the pressure at the base of the pool P_p (Eq. (17));
#6) Calculate the average hydrostatic temperature difference ΔT_h (Eq. (15));
#7) Calculate ΔT_a (Eq. (14));
#8) Calculate q_e (Eq. (13));
#9) Calculate R_3 (Eq. (11)), R_7 (Eq. (18)), R_{10} (Eq. (19)), and $R_{th,design}$ (Eq. (2));
#10) Calculate the thermal load value, q_{td} (Eq. (1));
#11) Compare q_{td} and q_e. If the values are too far apart, assume that q_{td} corresponds to the new value of q_e and repeat the steps from step #9) until the values of q_{td} and q_e converge.

From temperature results, other parameters were calculated. The experimental thermal resistance (R_{th}) of the thermosyphon was calculated by Eq. (23), in which T_{co} consists in the external temperature of condenser's wall, and q_{ps} represents the heat load provided by the power supply. The thermal efficiency (η_{th}) was calculated by Eq. (24), in which $\dot{m}_w$ represents the water mass flow at the condenser, and c_p the water specific heat. All properties were taken at the average temperature between T_{in} and T_{out}. Finally, the exergy efficiency (ε) was calculated by Eq. (25) (Jafarkazemi et al., 2016), in which T_a represents the ambient temperature, T_{out} and T_{in} consist in the outlet and inlet water's temperature, respectively.

$$R_{th} = \frac{T_{eo} - T_{co}}{q_{ps}} , \tag{23}$$

$$\eta_{th} = 100 \frac{\dot{m}_w c_p (T_{out} - T_{in})}{q_{ps}} , \tag{24}$$

$$\varepsilon = \frac{\dot{m}_w c_p \left[(T_{out} - T_{in}) - T_a \left(\ln \frac{T_{out}}{T_{in}} \right) \right]}{q_{ps} \left[1 - \left(\frac{T_a}{T_{eo}} \right) \right]} 100 . \tag{25}$$

The convective coefficient $h_{o,cond}$ from Eq. (4) was determined using Churchill and Bernstein (1977) correlation for the *Nusselt* number for external cross flow in cylinders (Eq. (26)). The parameter l_{cond} that was really in contact with flowing water was 85mm, and that is the value used for the calculations at the thermal design.

$$\bar{N}u_D = \frac{h_{o,cond} d_o}{k} = 0.3 + \frac{0.62 \, \mathrm{Re}_D^{1/2} \, \mathrm{Pr}^{1/3}}{\left[1 + (0.4 / \mathrm{Pr})^{2/3} \right]^{1/4}} \left[1 + \left(\frac{\mathrm{Re}_D}{282,000} \right)^{5/8} \right]^{4/5} . \tag{25}$$

4. RESULTS AND DISCUSSION

Figure 4 presents the temperature distribution versus time for all the four heat loads applied to the thermosyphon. As it can be seen, at the heat load of 80W there were some temperature peaks at the evaporator region. These peaks occur due the fact that this region is not totally filled with the working fluid, since the filling ratio is 50%. In that way, the regions that are filled with the working fluid have a higher mass that needs to be heated, taking longer to heat than regions not filled with working fluid. Therefore, until the evaporation and condensation processes start, regions with no working fluid will achieve higher temperatures. When the working fluid returns from the condenser to the evaporator, the temperatures stabilize until they reach steady state.

In general, the temperature distribution behaved as expected. When a heat load was applied, temperatures started to rise until the device reached the steady state. Evaporator's temperature was higher than adiabatic's temperature, which was also higher than condenser's temperature. Higher heat loads resulted in higher temperatures at each section of the device, and outlet water's temperature was higher than inlet temperature. All these facts may indicate that the device is working properly.

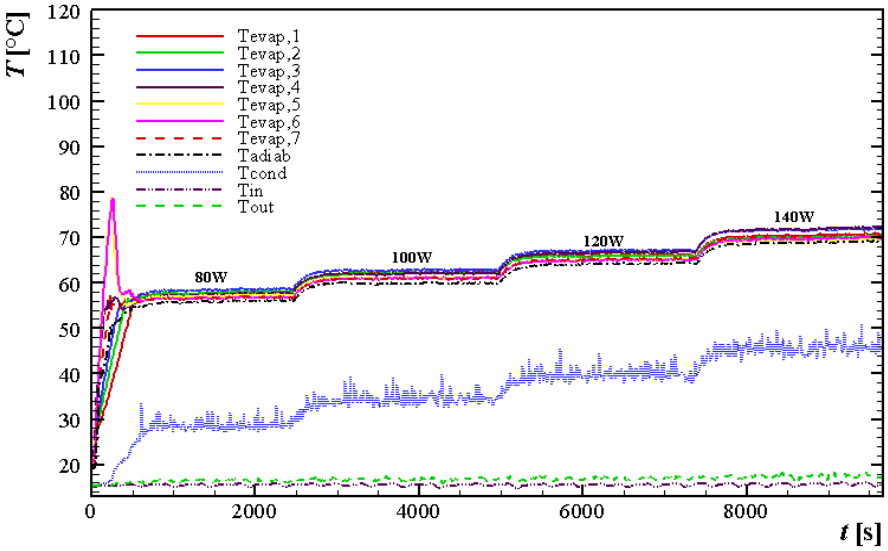

Figure 4. Temperature distribution.

Figure 5 presents results of thermal resistance (R_{th}) versus heat load (q_{ps}). The experimental uncertainties are due to the thermocouples (±1.27°C), power supply's current (±0,003A) and tension (±0,003V), and flow rate (±0,0000015 m³/s). The resulting uncertainties were calculated from *EES*™. From Figure 5 it can be seen that higher heat loads resulted in lower thermal resistance. That result was also expected and indicates the proper working of the device, since in Eq. (23) thermal resistance is inversely dependent of heat load, and so higher heat load should lower the values of R_{th}.

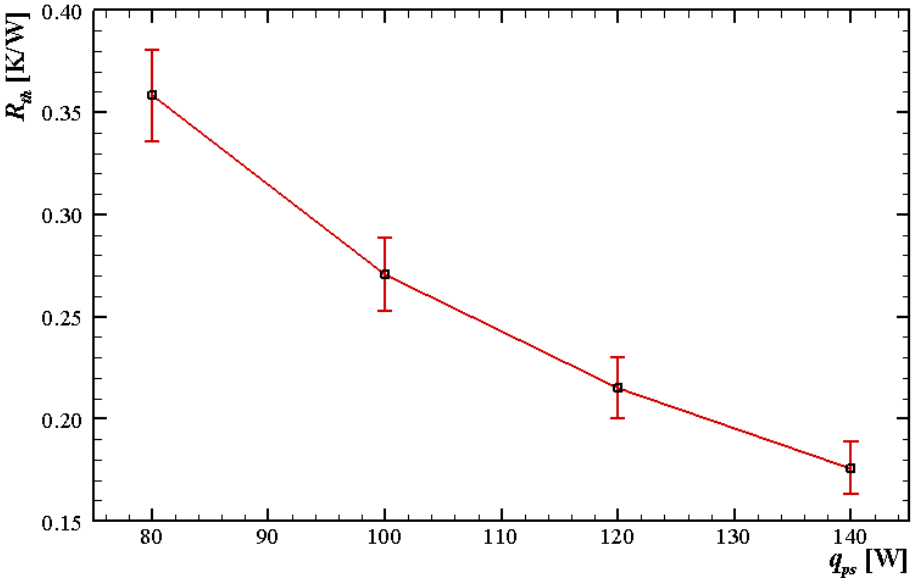

Figure 5. Thermal resistance.

Figure 6 presents the results from the thermal load calculated from the thermal design (q_{td}) versus the heat load applied to the power supply (q_{ps}).

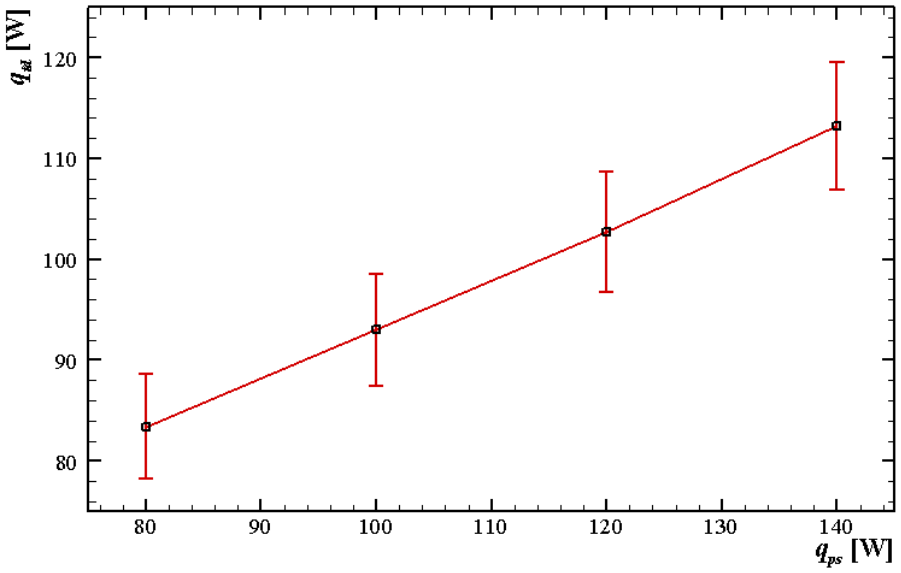

Figure 6. Thermal design results.

Figure 6 shows that the tendency between all data is almost a straight line, which may indicate a correspondence between the values calculated. The thermal design result for the 80W heat load was higher than the heat load itself applied, but, considering the uncertainties, this result is acceptable. It is possible to notice that the increase of heat load increases the difference from the heat load value and the thermal design result. This can be justified from the fact that the experimental condition is not an ideal insulation, and since at higher heat loads higher is the difference between the device temperature and the ambient temperature, the higher is the heat exchange and consequently the higher the heat loss.

Table 1 presents values of heat transferred to the flowing water (q_w), thermal and exergy efficiency for each heat load.

Table 1. Efficiency results.

q_{ps} [W]	q_{td} [W]	q_w [W]	η_{th} [%]	ε [%]
80.2	83.4	54.5	67.9	0.13
100.8	93.0	70.9	70.4	0.42
120.4	102.7	87.2	72.4	0.57
140.1	113.2	105.7	75.5	1.05

Table 1 shows that higher heat loads result in higher thermal and exergy efficiencies. It also can be seen there were heat losses from the heat exchange between the condenser and the flowing water. This may result from the fact that the cross section of the tee is considerably higher than the area of the condenser, in that way, between the condenser and the temperature acquisition spot, heated water can be mixed with non-heated water, lowing its temperature. The low exergy efficiency can also be justified by the fact that the inlet water temperature is kept at the same ambient temperature, and, since exergy considers the available energy in comparison with the “dead state” (ambient temperature), a low difference between the fluid’s temperature and the ambient temperature results in a low exergy efficiency.

There are few points in the experimental apparatus that can be improved in order to achieve better results, such as improving the insulation of the adiabatic section and the evaporator and also using insulation at the manifold, which was not used in this study. Besides that, thermocouples can be calibrated in order to reduce the experimental uncertainties. Tests in a real condition, where water inlet temperature is not kept constant can also be performed. A new manifold can also be developed, with a more restrict cross section area that fits the condenser area properly. All these actions may result in lower heat losses and, consequently, higher thermal and exergy efficiencies.

Besides that, considering all the results, the thermosyphon operated satisfactorily and according to the expected results, showing that the methodology used to its construction is adequate and can be used to build more thermosyphons to be used in a PV/T system composed by a photovoltaic panel and thermosyphons.

5. CONCLUSIONS

In this present work, a thermosyphon was developed and its experimental performance was compared with its thermal design. The thermosyphon was manufactured from a copper ASTM B75 tube with an outer diameter of 22.23mm, an inner diameter of 20.80mm, and a total length of 840mm. The working fluid used was distilled water with a filling ratio of 50% of the evaporator volume. The evaporator has a length of 650mm, while the adiabatic section and condenser have lengths of 80mm and 110mm, respectively. For the experimental test, heat was discharged in the evaporator region due to Joule's effect using a resistive tape and a power supply while heat was dissipated at the condenser region by means of a water flow of 0.9L/min. Heat loads of 80 to 140W were applied during the tests. Thermocouples were placed along the thermosyphons aiming to collect temperature data at the three regions of the passive device. Equations of the thermal design, parameters, and results from the experimental tests were implemented in a programming at *F-Chart*™ software *Engineering Equation Solver*™ (*EES*™), obtaining values of heat loads to be compared with the heat load applied to the thermosyphon. Some specific points of the experimental apparatus were identified for possible adjustments, such as better insulation, different manifold, and different water flow conditions. The thermosyphon operated as expected in all the analyzed aspects – temperature distribution, thermal resistance, thermal design's heat load, and thermal and exergy efficiencies – showing that the methodology used to its construction is adequate.

6. ACKNOWLEDGEMENTS

Acknowledgments are provided to the Capes, the CNPq, the PROPPG/UTFPR, the DIRPPG/UTFPR, the PPGEM/ UTFPR/PG, and the DAMEC/UTFPR/PG.

7. REFERENCES

Aguiar, V.M., 2016. *Influência da Razão de Preenchimento e da Inclinação no Desempenho Térmico de Termossifões*. Graduation work, Federal University of Technology – Paraná, Ponta Grossa, Brazil.

Akbasrzadeh, A. and Wadowski, T., 1996. "Heat pipe-based cooling systems for photovoltaic cells under concentrated solar radiation". *Applied Thermal Engineering*, Vol. 16, pp. 81–87.

Antonini Alves, T., Krambeck, L. and Santos, P.H.D., 2018. "Heat Pipe and Thermosyphon for Thermal Management of Thermoelectric Cooling". In: Aranguren, P. (Org.). *Bringing Thermoelectricity into Reality*. InTech, London, UK.

Churchill, S. W. and Bernstein, M. A., 1977. "A correlating equation for forced convection from gases and liquids to a circular cylinder in crossflow". *Journal of Heat Transfer*, Vol. 99, No. 2, pp. 300–306.

Groll, M. and Rösler, S., 1992. "Operation principles and performance of heat pipes and closed two-phase thermosyphons". *Journal of Non-Equilibrium. Thermodynamics*, Vol. 17, No. 2, pp. 91–151.

Jafarkazemi, F., Ahmadifard, E. and Abdi, H., 2016. "Energy and exergy efficiency of heat pipe evacuated tube solar collectors". *Thermal Science*, Vol. 20, No. 1, pp. 327–335.

Mantelli, M.B.H., 2013. "Thermosyphon Technology for Industrial Applications". In: Vasiliev, L.L. and Kakaç, S. (Eds.). *Heat Pipes and Solid Sorption Transformations: Fundamentals and Practical Applications*. CRC Press, Boca Raton, USA.

Peterson, G. P., 1994. *An Introduction to Heat Pipes: Modeling, Testing and Application*. John Wiley & Sons, New York, USA.

Reay, D.A., Kew, P.A. and McGlen, R.J., 2014. *Heat Pipe: Theory, Design and Applications*. Butterworth-Heinemann, Amsterdam, NED.

8. RESPONSIBILITY NOTICE

The authors are the only responsible for the printed material included in this paper.